Stochastic Calcium Oscillations

James P. Keener
Department of Mathematics
University of Utah
Salt Lake City, UT 84112

April 18, 2006

Keywords: calcium dynamics, stochastic release, spark to wave transition, IP_3 receptors, fire-diffuse-fire model

Abstract

While the oscillatory release of calcium from intracellular stores is comprised of fundamentally stochastic events, most models of calcium oscillations are deterministic. As a result, the transition to calcium oscillations as parameters, such as IP_3 concentration, are changed, is not described correctly. The fundamental difficulty is that whole cell models of calcium dynamics are based on the assumptions that the calcium concentration is spatially homogeneous, and that there are a sufficiently large number of release sites per unit volume so that the law of large numbers is applicable. For situations where these underlying assumptions are not applicable, a new modeling approach is needed.

In this paper we present a model and its analysis of calcium dynamics that incorporates the fundamental stochasticity of release events. The model is based on the assumptions that release events are rapid, while reactivation is slow.

The model presented here is comprised of two parts. In the first, a stochastic version of the fire-diffuse-fire model is studied in order to understand the spark-to-wave transition and the probability of sparks resulting in abortive waves vs. whole cell calcium release. In the second, this information about the spark-to-wave transition is incorporated into a stochastic model (a Chapman-Kolmogorov equation) that tracks the number of activated and inactivated calcium release sites as a function of time. By solving this model numerically, information about the timing of whole cell calcium release is obtained. The results of this analysis show a transition to oscillations that agrees well with data and with Monte Carlo simulations.

Acknowledgment: This research was supported in part by NSF Grant DMS-0211366.

1 Introduction

It is now well established that release of calcium from internal calcium stores into the cellular cytoplasm is via events that are fundamentally stochastic in nature [3, 22, 32]. In fact, all ion

channels have the feature that they are either open or closed, conducting or non-conducting, with opening and closing describable as Markov processes. Mathematical models of the dynamics of cellular events such as calcium release or action potentials have not utilized fully stochastic descriptions because of the implicit assumption that the law of large numbers is applicable, and that the ensemble of stochastic channels can be described by their average behavior. However, it is now understood that for calcium, at least, this assumption may not be valid in many physiological conditions.

Calcium channels such as IP_3 receptors (IPR) and ryanodine receptors (RYR) have the added feature that they are regulated by the local concentration of calcium [32]. Since the concentration of calcium in the vicinity of the release channel can be substantially different than the whole cell average calcium concentration [27, 29], i.e., since the calcium that is released by the receptor does not immediately diffuse into the whole cell, a model that uses only whole cell calcium is limited in its ability to faithfully describe calcium dynamics [30].

The need for an understanding of the stochastic nature of calcium release is illustrated by the observed onset of whole cell calcium oscillations as $[IP_3]$ is increased in *Xenopus* oocytes [21]. At low $[IP_3]$ only puffs are observed; there is not enough Ca^{2+} released from a cluster to stimulate Ca^{2+}release from neighboring sites, so the calcium transient is purely local. However, as $[IP_3]$ is increased, both the sensitivity of and the amount of Ca^{2+} released from each IPR increases. This allows for the development of waves that emerge from a nucleation site. However, at moderate levels of $[IP_3]$, global events are rare and in many cases there are waves that progress only a short distance before dying out. In this situation, both the average time between whole cell release events and its standard deviation are large, and are decreasing as $[IP_3]$ increases. Finally, at high $[IP_3]$, global waves are seen to occur regularly with a well-defined period.

Whole cell models for calcium dynamics typically are of the form [11, 28]

$$\frac{dc}{dt} = J_{rel} - J_{uptake}, \tag{1}$$

where c is the cytoplasmic concentration of calcium, J_{rel} is the flux (in units of concentration per unit time) of calcium into the cytoplasm through release from calcium stores, and J_{uptake} is the flux of calcium via uptake into the calcium stores. The release flux J_{rel} typically takes the form

$$J_{rel} = gP_o(c_e - c), \tag{2}$$

where g is the maximal conductance, P_o is the open probability, and $c_e - c$ is the channel driving force, which is governed by the difference between ER (endoplasmic reticulum) calcium c_e, and cytoplasmic calcium c. In light of our introductory comments, a more accurate model would take into account the stochastic and spatial nature of the receptors and use

$$\frac{\partial c}{\partial t} = D\nabla^2 c + \sum_k \delta(x - x_k) J^k_{rel} - J_{uptake}, \tag{3}$$

where x_k represents the spatial location of single channels or small clusters of channels, and J^k_{rel} represents the release of calcium from the k^{th} release unit. Furthermore,

$$J^k_{rel} = g_k p_k (c_e - c), \tag{4}$$

where p_k is a random variable with values zero or one to indicate whether the release unit is closed or open. One obtains the whole cell model (1) in the limit that diffusion is large compared to the total size of the cell *and* that there are a sufficiently large number of release sites so that the random variables p_k can be replaced by the ensemble average open probability P_o. As mentioned above, there is growing evidence that these assumptions are not valid in many physiological situations, such as oocytes. (A similar challenge exists for the emergence of synchronized bursting in pancreatic beta cells [24, 25].)

So far, the only way around these difficulties has been to use Monte Carlo simulations [2, 9, 10]. While these capture the essential random behavior of release events, and give results that correspond to the data, they suffer from the fact that they are computationally expensive, and there is no realistic possibility of extending them to multicellular settings.

The goal of this paper is to develop a model of calcium dynamics that takes into account the stochastic nature of release without relying solely on large scale Monte Carlo simulations, thereby keeping the computational cost much more manageable, and at the same time providing some analytical understanding of this stochastic process. Of course, to do so requires that some approximations be made.

The fundamental assumption to be made in this analysis is that calcium release and recovery occur on two different time scales. To see the basis for this assumption, consider a typical example of whole cell models,

$$\frac{dc}{dt} = (k_f P_o + J_{er})(c_e - c) - J_{uptake}, \tag{5}$$

where

$$J_{uptake} = \frac{c - \alpha_1 c_e}{\alpha_2 + \alpha_3 c + \alpha_4 c_e + \alpha_5 c c_e}, \tag{6}$$

$$P_o = \left(\frac{pch}{(p+K_1)(c+K_5)}\right)^3, \tag{7}$$

$$\frac{dh}{dt} = \phi_2(1-h) - \phi_1 h, \tag{8}$$

$$c_e = \frac{1}{\gamma}(c_T - c), \tag{9}$$

and

$$\phi_1 = \frac{(k_{-4}K_2K_1 + k_{-2} + pK_4)c}{K_4K_2(p+K_1)}, \tag{10}$$

$$\phi_2 = \frac{k_{-4}p + k_{-2}K_3}{p+K_3}, \tag{11}$$

$K_j = \frac{K_{-j}}{k_j}, j = 1, \cdots, 5$. Parameter values are given in Table 1.

Here, c represents the whole cell calcium concentration, h is the IPR inactivation variable, and p represents the IP_3 concentration. The parameters used here for the dynamics of the inactivation variable h and the open probability P_o are based on the Keizer-DeYoung 8-state receptor model [17, 33] found using a quasi-steady state approximation [16, 20], while the parameters for J_{uptake} are based on the work of [12].

k_1	=	400 $\mu M^{-1}s^{-1}$	k_{-1}	=	52 s^{-1}
k_2	=	0.2 $\mu M^{-1}s^{-1}$	k_{-2}	=	0.21 s^{-1}
k_3	=	400 $\mu M^{-1}s^{-1}$	k_{-3}	=	377.2 s^{-1}
k_4	=	0.2 $\mu M^{-1}s^{-1}$	k_{-4}	=	0.029 s^{-1}
k_5	=	20 $\mu M^{-1}s^{-1}$	k_{-5}	=	1.64 s^{-1}
α_1	=	10^{-4}	α_2	=	0.007 s
α_3	=	0.06 μM^{-1}s	α_4	=	0.0014 μM^{-1}s
α_5	=	0.007 μM^{-2}s	J_{er}	=	0.002 s^{-1}
k_f	=	0.96 s^{-1}	γ	=	5.5

Table 1: Parameter values of the model of calcium dynamics (5)-(8).

The numerical solution of this model with $p = 2$ and $c_T = 10\mu$M is shown in the upper panel of Figure 1. The phase portrait for this same trajectory is shown in the lower panel, with calcium plotted on a logarithmic scale on the horizontal axis, and h plotted on the vertical axis. The nullcline for h is monotone decreasing as a function of c, while the nullcline for c is n-shaped; both are shown dashed. The trajectory in the lower panel is shown with circular dots plotted at equal time steps of 0.1 s.

These simulations illustrate the time scale separation. The time constant for h is a function of c and varies from below 1s when calcium is high to greater than 10s when calcium is low. Calcium release occurs when h reaches a threshold, calcium is rapidly released, and h quickly inactivates. In the subsequent slower phase, h gradually increases until another release event is initiated.

The behavior of this model as a function of $[IP_3]$ is also stereotypical of whole cell calcium models. At small $[IP_3]$ levels, there is a globally stable steady state solution with little calcium. As $[IP_3]$ is increased, there is a subcritical Hopf bifurcation which is connected through a saddle-node bifurcation to a large amplitude stable periodic solution, an example of which is depicted in Fig. 1. Unfortunately, this description of the onset of oscillations is not consistent with the experimental data described above.

In what follows, we study the dynamics of calcium oscillations by examining first the fast release event, and then the slow recovery phase, which, pieced together gives a stochastic interpretation of the onset of calcium oscillations. First, a stochastic version of the fire-diffuse-fire model is used to develop a renewal equation whose solutions describe the spark-to-wave transition. From this, analytical formulas for the probability that sparks result in abortive waves or whole cell calcium release are developed. Second, this information about the spark-to-wave transition is incorporated into a stochastic model (a Chapman-Kolmogorov equation) that tracks the number of activated and inactivated calcium release sites as a function of time. By solving this model numerically, information about the timing of whole cell calcium release is obtained.

2 Calcium Release - The Spark to Wave Transition

Experiments [21] clearly show that whole cell calcium release is initiated by the rapid release of calcium from a small localized cluster of channels, which then propagates to the entire cell. In fact, there are three types of response to a single release event: the neighboring release sites may remain quiescent, the neighboring sites may also release calcium but the attempt to engage the entire cell is abortive, or the neighboring sites may release calcium which in turn stimulates their neighbors, and so on, until calcium sites throughout the entire cell have released calcium [15, 18].

The fact that release sites are discrete in space makes it reasonable to examine the popular fire-diffuse-fire model, [8, 19, 23]

$$\frac{\partial c}{\partial t} = D\frac{\partial^2 c}{\partial x^2} - k_s c + \sigma \sum_n \delta(x - x_n)\delta(t - t_n). \tag{12}$$

Here we assume that the cell is one-dimensional, with release sites separated by the fixed distance L, so that $x_n = nL$. (The distance between sites could also be taken to be randomly distributed, as in [2].) The parameter σ represents the total amount of calcium released in a single release event from a single cluster. We represent the release site geometry using a delta function in space since clusters have a diameter of 60-100 nm, while the distance between clusters is 3-7 μm [21]. The term $k_s c$, which is not included in many early discussions of the fire-diffuse-fire model, is included here to model spatially continuous uptake via SERCA exchange pumps. Linear uptake was included in the treatment of the fire-diffuse-fire model given in [4].

The assumption that the cell is one-dimensional is perhaps more appropriate for cardiac cells than for cell with IPR's. However, the fundamental discreteness of release events is well-captured by a one-dimensional model. The primary difference between one and two-dimensional arrays of release sites is that it is relatively easy for a wave to terminate in one-dimension, whereas in two dimensions it is possible for a calcium wave to move around and bypass inactive release sites. In this way, it is possible for a calcium wave to propagate throughout an entire cell without participation from all release sites. A one-dimensional model does not have this capability.

The advantage of using equation (12) to model the release and spread of calcium is that the local calcium concentration can be calculated analytically if the release times are known. For example, the calcium that is released at site x_j and time t_j is distributed throughout space according to

$$c_j(x,t) = \sigma \frac{H(t - t_j)}{\sqrt{4\pi D(t - t_j)}} \exp\left(-\frac{(x - x_j)^2}{4D(t - t_j)} - k_s(t - t_j)\right), \tag{13}$$

where H is the usual Heaviside function. (Here we assume that the cell is large enough so that boundary conditions can be safely ignored.) Because the equation for c is linear, the full solution is the linear superposition of released calcium,

$$c(x,t) = \sum_k c_k(x,t). \tag{14}$$

The only place where $c(x,t)$ needs to be evaluated is at a release site. At the k^{th} release site the calcium from site j is

$$c_j(x_k,t) = \frac{\sigma}{L} C_{j,k}(t), \tag{15}$$

with

$$C_{j,k}(t) = \frac{H(t-t_j)}{\sqrt{4\pi\delta k_s(t-t_j)}} \exp\left(-\frac{(k-j)^2}{4\delta k_s(t-t_j)} - k_s(t-t_j)\right), \tag{16}$$

where $\delta = \frac{D}{k_s L^2}$ is a dimensionless diffusion parameter.

It is easy to modify the fire-diffuse-fire model so that release is not instantaneous but occurs over some specified time interval, as was assumed in [6]. The main effect of this modification is to change the details of the fundamental solution $C_{j,k}(t)$. However, once the fundamental solution is tabulated, it can be used in the subsequent analysis with no further modification. Further, in principle, this same analysis could be applied in a two dimensional medium, since all that is needed is the radially symmetric fundamental solution of the diffusion equation, which is also easily tabulated.

With $D = 20\mu\text{m}^2/\text{s}$ [1], $L = 2\mu\text{m}$, and $k_s = \frac{1}{\alpha_2} = 0.007\text{s}$ (see Table 1), we estimate that $\delta = 0.035$ (the length constant is 0.4 μm). (In *Xenopus* oocytes, IPR clusters have a density of about 1 per $30\mu\text{m}^2$, for an average separation of about 5.5 μm.) As we will see, with δ this small, the analysis of the spark-to-wave transition is simplified substantially. However, to cover all the bases, we will examine solutions for larger values of δ as well.

Plots of the function $C_{0,k}(t)$ are shown in Fig. 2, plotted in units of dimensionless time $k_s t$ with $\delta = 2.0$ for $k = 1, 2, 3$, and 4. These plots depict the transient calcium concentration at the four nearest neighbors to a release site following release at time $t = 0$. It is noteworthy that the maximal amount of calcium at each of the sites is decreasing as a function of distance from the initial release site. This decrease is more substantial for smaller values of δ, and for $\delta = 0.035$, the maximal level of calcium at site 2 is 0.0033 times the maximal level of calcium at site 1.

In the deterministic version of the fire-diffuse-fire model, t_n is determined as the first time at which the local calcium level reaches a specified threshold, say θ. Here we assume that the release is not a deterministic function of local calcium concentration but rather is a stochastic process. Thus, we assume that t_n is a random variable with cumulative probability $P_n(t)$, so that $P_n(t)$ is the probability that release from site x_n at time t_n occured before time t,

$$P_n(t) = P(t > t_n). \tag{17}$$

It follows that

$$\frac{dP_n}{dt} = k_{open}(c(x_n,t))(1-P_n), \qquad P_n(0) = 0, \tag{18}$$

where $k_{open}(c)$ represents the rate constant of channel opening as a function of the local calcium concentration. Notice that the probability that release occurs is $\lim_{t\to\infty} P_n(t) \equiv P_n^\infty$, and it may be less than one. Note also that $P_n(t)$ is different than the open probability that is often used in whole cell deterministic models, as there is no accounting for closing or inactivation in (18). In this model, the release from a single site is assumed to occur instantaneously, so no accounting of inactivation is neccessary. By definition, the probability

distribution function for the random variable t_n is

$$p_n(t) = \frac{dP_n}{dt}, \tag{19}$$

so that

$$p_n(t) = k_{open}(c(x_n, t)) \exp\left(- \int_0^t k_{open}(c(x_n, \eta)) d\eta \right). \tag{20}$$

Notice that $p_n(t)$ is not necessarily a true probability distribution function since $\int_0^\infty p_n(t)dt = P_n^\infty$ may be less than one. However, if we define $p_n(t|n)$ to be the distribution of release times for the n^{th} site given that a release event occurred at the n^{th} site, then

$$p_n(t|n) = \frac{p_n(t)}{P_n^\infty}, \tag{21}$$

and the expected time of firing is

$$E(t_n) = \frac{1}{P_n^\infty} \int_0^\infty t p_n(t) dt. \tag{22}$$

The structure of k_{open} is important. We expect that k_{open} is small when calcium concentration is small, and that it increases to become quite large if calcium concentration is high. In the deterministic limit,

$$k_{open} = \left\{ \begin{array}{ll} 0 & c < \theta \\ \infty & c > \theta \end{array} \right\}, \tag{23}$$

so that $P_n(t) = 0$ when $c(t) < \theta$, while $P_n(t) = 1$ after c has first reached and passed the threshold θ. Equivalently, in the deterministic limit, $p_n(t) = \delta(t - t_n)$.

A simple continuous extension of this is to take k_{open} to be the Hill function

$$k_{open}(c) = k_{max} \frac{c^N}{\theta^N + c^N}, \tag{24}$$

for some fixed value of N. This form for k_{open} was also used in [15] for cardiac cells. In the limit of large N, k_{open} approaches the Heaviside function $k_{max} H(c - \theta)$.

Now suppose that there is a calcium release event at site 0 at time $t = 0$. We want to determine the probability that this single release event leads to a whole cell response. However, whole cell release requires the sequential calcium release from a large number of individual sites. So, first, we must determine the response of neighboring sites to the initial release event.

The probability of release at a neighboring site is related to the calcium transient at that site, depicted in Fig. 2. If there has been only one release event (at site 0), then the cumulative probability function for time of release from another site is given by (18), where $c(x_n, t) = \frac{\sigma}{L} C_{0,n}(t)$.

Fig. 3 shows examples of the function $p_1(t)$ for several values of release amount $\frac{\sigma}{\theta L}$. Fig. 4 shows the probability of firing at site 1 (P_1^∞) as a function of the parameter $\frac{\sigma}{\theta L}$. For both of these plots, k_{open} is specified by (24) with $k_{max} = 200 k_s$, $N = 4$. Plots of the moments m_0, m_1 and m_2 where

$$m_k = \int_0^\infty t^k p_1(t) dt, \tag{25}$$

are shown plotted as a function of $\frac{\sigma}{\theta L}$ in Fig. 5, and the mean and variance of the distribution $\frac{p_1(t)}{P_n^\infty}$ are shown plotted in Fig. 6, here for $\delta = 0.1$.

It should come as no surprise that the expected time of firing (the mean) at site one is a decreasing function of $\frac{\sigma}{\theta L}$. It is also noteworthy that as $\frac{\sigma}{\theta L}$ increases the variance of the release time decreases to zero, indicating that release becomes more deterministic in this limit.

To calculate the probability of release at site n we must know the time evolution of calcium concentration at site n, and this requires knowing the previous times of release at other sites. It simplifies the situation substantially if release is always sequential, proceeding from site 1 to site 2 to site 3, and so on. To check if this is the case, we examine the probability that site $n > 1$ releases before site 1. We calculate that if there is release from site 1, the (conditional) probability that site 1 releases before site n (even if site n does not release) is

$$P(t_1 < t_n | \text{site 1 release occurs}) = P_n^\infty \int_0^\infty \int_0^{t_n} \frac{p_1(t_1)}{P_1^\infty} \frac{p_n(t_n)}{P_n^\infty} dt_1 dt_n + 1 - P_n^\infty \quad (26)$$

$$= \frac{1}{P_1^\infty} \int_0^\infty P_1(t_n) p_n(t_n) dt_n + 1 - P_n^\infty, \quad (27)$$

and the probability that there is release from site n and not from site 1 is $P_n^\infty(1 - P_1^\infty)$. These quantities are easy to compute numerically. These computations show that if k_{open} has a transition near $c = \theta$ that is sufficiently sharp, then the probability of sequential release is close to one. In Fig. 4, the upper unlabeled curve (shown dashed) is the probability that firing at site 1 precedes firing at site 2, given that firing occurs at site 1. Thus, when there is sufficient cooperativity for release, the probability that release is out of sequence is quite small. Furthermore, the probability that release is out of sequence decreases as δ decreases.

Now we calculate the probability of release at site n. If the release time from all previous sites is known, then the time course of the calcium concentration at site n is known,

$$c(x_n, t) = \frac{\sigma}{L} \sum_{j=0}^{n-1} C_{j,n}(t - t_j), \quad (28)$$

where $t_0 = 0$, and the conditional cumulative probability function $P_n(t_n | t_{n-1}, \cdots, t_0)$ is the solution of (18) with $c(x_n, t)$ given by (28).

In spite of the fact that P_n shows dependence on all previous firing times, this dependence is exponentially decreasing in its importance, and so significant simplifications are possible, depending on the size of the diffusion parameter δ. To see the relative importance of the previous firing times, we examine the relative amplitudes of the individual terms comprising the sum (28) $\frac{a_j}{a_1}$, where

$$a_j = \max_t C_{0,j}(t). \quad (29)$$

In Fig. 7, the ratios $\frac{a_2}{a_1}$ and $\frac{a_3}{a_1}$ are plotted as functions of δ on a log-log plot. Observe that for small δ, these ratios are quite small, suggesting that we can ignore all but the most recent firing time.

In this case, it follows that

$$p_n(t) = \int_0^t p_n(t|t_{n-1}) p_{n-1}(t_{n-1}) dt_{n-1}. \tag{30}$$

However, because it depends only on the time of firing of its immediate neighbor, $p_n(t|t_{n-1}) = p_1(t - t_{n-1})$ and (30) can be rewritten as

$$p_n(t) = \int_0^t p_1(t-s) p_{n-1}(s) ds. \tag{31}$$

Equation (31) is a standard renewal equation about which much can be determined [7]. For example, the zeroth moment of $p_n(t)$ is

$$\begin{aligned} P_n^\infty = \int_0^\infty p_n(t) dt &= \int_0^\infty \int_0^t p_1(t-s) p_{n-1}(s) ds dt, \\ &= \int_0^\infty \int_s^\infty p_1(t-s) p_{n-1}(s) dt ds, \\ &= \int_0^\infty \int_0^\infty p_1(t) p_{n-1}(s) dt ds, \\ &= \left(\int_0^\infty p_1(t) dt \right) \left(\int_0^\infty p_{n-1}(t) dt \right), \\ &= m_0^n, \end{aligned} \tag{32}$$

where $m_0 = P_1^\infty$ is the zeroth moment of $p_1(t)$. Similarly, the first moment of $p_n(t)$ is

$$\begin{aligned} \int_0^\infty t p_n(t) dt &= \int_0^\infty \int_0^t t p_1(t-s) p_{n-1}(s) ds dt, \\ &= \int_0^\infty \int_s^\infty t p_1(t-s) p_{n-1}(s) dt ds, \\ &= \int_0^\infty \int_0^\infty (t+s) p_1(t) p_{n-1}(s) dt ds, \\ &= \int_0^\infty t p_1(t) dt \int_0^\infty p_{n-1}(s) ds + \int_0^\infty p_1(t) dt \int_0^\infty s p_{n-1}(s) ds, \\ &= m_1 m_0^{n-1} + m_0 \int_0^\infty s p_{n-1}(s) ds, \end{aligned} \tag{33}$$

where $m_1 = \int_0^\infty t p_1(t) dt$ is the first moment of $p_1(t)$. It follows that $\int_0^\infty t p_n(t) dt = n m_1 m_0^{n-1}$.

By a similar calculation, it can be shown that

$$\int_0^\infty t^2 p_n(t) dt = n m_2 m_0^{n-1} + n(n-1) m_1^2 m_0^{n-2}, \tag{34}$$

where $m_2 = \int_0^\infty t^2 p_1(t) dt$ is the second moment of $p_1(t)$.

From these calculations it follows that the mean of the probability distribution function $\frac{p_n(t)}{P_n^\infty}$ is $n \frac{m_1}{m_0}$ and its variance is $n \left(\frac{m_2}{m_0} - (\frac{m_1}{m_0})^2 \right)$. As a result, the ratio $\frac{m_1}{m_0}$ is the expected

site-to-site delay, the inverse of the wave speed. Not surprising, the site-to-site delay is a decreasing function of $\frac{\sigma}{\theta L}$. Notice also that the variance is also a decreasing function of $\frac{\sigma}{\theta L}$, indicating that for larger $\frac{\sigma}{\theta L}$, propagation becomes "more deterministic".

Figs. 8 and 9 show the sequence of functions $p_n(t)$ for $\delta = 0.1$ and $\frac{\sigma}{\theta L} = 3.5$ (Fig. 8) and $\frac{\sigma}{\theta L} = 6.5$ (Fig. 9). In the first of these two cases, $\frac{\sigma}{\theta L}$ is too small to allow propagation. Since $m_0 = 0.36$, there is but a 36% chance of release from the first site, and m_0^n approaches zero quickly, so that the probability of subsequent release events is quite small. On the other hand, in the second case, a steadily propagating wave is quickly established.

The probability of release from the n^{th} site P_n^∞ is the same as the probability that the extent of propagation (denoted N_e) is greater than or equal to n,

$$P(N_e \geq n) = P_n^\infty. \tag{35}$$

It follows that

$$P(N_e = n) = P_n^\infty - P_{n+1}^\infty, \tag{36}$$

and the expected extent of propagation is

$$E(N_e) = \sum_n n(P_n^\infty - P_{n+1}^\infty) = \sum_{n=1}^\infty P_n^\infty. \tag{37}$$

In the case calculated above where $P_n^\infty = m_0^n$, we find that

$$P(N_e = n) = m_0^n(1 - m_0), \tag{38}$$

and

$$E(N_e) = \frac{m_0}{1 - m_0}. \tag{39}$$

Fig. 10 shows the expected number of release events as a function of $\frac{\sigma}{\theta L}$. This curve characterizes the spark-to wave-transition. While there is no true threshold for this transition, it is seen that for $\frac{\sigma}{\theta L}$ small, the expected number or release events is less than one, a spark, while for $\frac{\sigma}{\theta L}$ sufficiently large, a wave is essentially certain.

The shape of the functions $p_n(t)$ seen in Figs. 8 and 9 suggests that there are some easy solutions of the recurrence equation (31). Indeed, it is easy to show that if $p_1(t) = A_1 t^\alpha \exp(-\lambda t)$, then $p_n(t) = A_n t^{n\alpha+n-1} \exp(-\lambda t)$, for appropriately chosen coefficients A_n. For example, if $\alpha = 0$, then $p_1(t)$ is an exponential distribution, and (31) generates the Poisson distribution. The general solution of (31) can also be found using Laplace Transforms.

All of the previous calculations of $p_n(t)$ relied on the assumption that release at a given site is influenced only by the calcium released from its nearest neighbor, an assumption that is valid only if δ is sufficiently small ($\delta \leq\sim 0.1$). For larger values of δ it may be necessary to include the effect of more sites. For example, if the nearest two sites are significant

$$\begin{aligned} p_n(t) &= \int_0^t \int_0^t p_n(t|t_{n-1}, t_{n-2}) p_{n-1}(t_{n-1}) p_{n-2}(t_{n-2}) dt_{n-1} dt_{n-2} \\ &\quad + (1 - P_{n-2}(t)) \int_0^t p_n(t|t_{n-1}, \sim t_{n-2}) p_{n-1}(t_{n-1}) dt_{n-1} \end{aligned}$$

$$
\begin{aligned}
&+(1-P_{n-1}(t))\int_0^t p_n(t|\sim t_{n-1},t_{n-2})p_{n-2}(t_{n-2})dt_{n-2}\\
=\;&\int_0^t\int_0^t p_2(t|t_1,t_0)p_{n-1}(t_1)p_{n-2}(t_0)dt_1dt_0\\
&+(1-P_{n-2}(t))\int_0^t p_2(t|t_1,\sim t_0)p_{n-1}(t_1)dt_1\\
&+(1-P_{n-1}(t))\int_0^t p_2(t|\sim t_1,t_0)p_{n-2}(t_0)dt_0, \qquad (40)
\end{aligned}
$$

where $p_2(t|t_1,t_0)$ is the firing time distribution for site 2 with release from site 1 at time t_1 and release at site 0 at time t_0, and $p_2(t|t_1,\sim t_0)$ is the firing time distribution for site 2 with release from site 1 at time t_1 and no release at site 0. Notice that if $p_2(t|t_1,t_0)$ is independent of t_0, then $p_2(t|t_1,t_0)=p_1(t|t_1)$. Then, if $p_2(t|\sim t_1,t_0)$ is also neglected, (40) reduces to (31). Notice that in this equation, we have not assumed that release is strictly sequential. The only assumption used here is that $C_{0,3}(t) << C_{0,1}(t)+C_{0,2}(t)$, i.e., that only the two nearest neighbors have a significant effect on release.

Fig. 11 shows a plot of $p_2(t|t_1,t_0=0)$ for 24 different values of t_1 ranging from 0 to $4.6k_s$, with t_1 increasing from left to right, with $\delta=1.0$. Noticeable is the effect of release from site zero when t_1 is small (the leftmost profiles) while when t_1 is large, the release at site 2 is independent of release at site 0. It is useful for computational purposes to note that

$$p_2(t|t_1,t_0)=p_2(t-t_0|t_1-t_0,0). \qquad (41)$$

Equation (40) does not have such easily computed solutions as does (31). However, the qualitative behavior of solutions of the two equations is the same.

Fig. 12 shows a sequence of solutions of (40) in the case that $\delta=1.0$. The sequence of dashed curves are the solutions of the recurrence equation (31). Clearly, for this value of δ, release at a given site is determined by the amount of calcium that is released from more than its nearest neighbor. In fact, while release from site one is identical for the two models, release from site two is enhanced markedly by release from site zero.

Fig. 13 shows the expected value of N_e, the extent of propagation, as defined in (37), plotted as a function of $\frac{\sigma}{\theta L}$ for $\delta=1$, calculated using solutions of (40). The dashed curve shows the expected value of N_e calculated using solutions of (31), which relies on the assumption that only nearest neighbor interactions are significant. Although these two curves are quantitatively different, they are qualitatively similar, showing the spark to wave transition as a function of $\frac{\sigma}{\theta L}$. All plots of $E(N_e)$ show the same qualitative behavior, namely that for small $\frac{\sigma}{\theta L}$, sparks do not propagate; for sufficiently large $\frac{\sigma}{\theta L}$, propagation extends throughout the entire medium; for intermediate parameter ranges, propagation is abortive.

3 Whole Cell Oscillations

The model of calcium oscillations developed here relies on the assumption that the primary events occur on two different time scales. On the fastest time scale is the release of calcium from a release site (or cluster of release sites), which then leads to a rapidly propagating

wave of release. Following this rapid release, recovery and return of excitability occurs on a slower time scale.

To model the slower events, we use an adaptation of the Keizer-DeYoung 8-state receptor model [17, 33]. According to this model, an IPR can be in any one of 8 states, denoted S_{ijk} with $i, j, k = 0, 1$. A subscript 1 indicates that a binding site is bound by its ligand and a zero subscript that it is unbound. The first subscript indicates binding with IP_3, the second with activating calcium, and the third with inactivating calcium. The conducting state is assumed to be S_{110}, and those sites in state S_{100} are activated, but not conducting. We also assume that the IP_3 concentration is fixed, so that the fraction of release sites that have IP_3 bound is some monotone increasing function of $[IP_3]$, for example $F([IP_3]) = \frac{[IP_3]}{K_p+[IP_3]}$. Now we focus our attention on those release sites in states S_{100}, S_{110}, S_{101}, and S_{111} (i.e., with $[IP_3]$ bound).

The effect of calcium release is to rapidly move a site from state S_{100} (the activated state) into S_{110} (the conducting state), then to S_{111} and thence to S_{101} (the inactivated state). The return of a site from the inactivated state S_{101} to the activated state S_{100} is assumed to be a slow (Markovian) process, with transition rate k_h. Since the transition from state S_{100} to state S_{101} mediated by calcium release is fast, we assume that sites are in either of the two states S_{100} or S_{101}.

Now we let h be the fraction of sites that are in state S_{100}, and $1-h$ to be the fraction of sites in state S_{101}. Since the transition from S_{101} to S_{100} is assumed to be a Markov process, the sites in each of these states are uniformly distributed throughout the cell - there can be no spatial correlation since an individual site can have no memory of how long it has been since it last had a release event.

We define $p(h, t)$ to be the probability distribution that the fraction of sites in state S_{100} is h at time t. The Chapman-Kolmogorov equation for the evolution of this probability is [14]

$$\frac{\partial p(h,t)}{\partial t} = -k_h \frac{\partial}{\partial h}\left((1-h)p(h,t)\right) - \beta M h p(h,t) + \int_h^1 W(\eta, h)p(\eta, t)d\eta. \tag{42}$$

Here β represents the rate at which a single activated site can have a spark, M is the total number of sites in states S_{100} and S_{101}, and $W(\eta, h)$ is the rate at which sites can (instantateously) jump from fraction η to fraction h. Thus, $W(\eta, h)$ represents the rate at which a spark causes the release of $M(\eta - h)$ sites, via an abortive wave. The function $W(\eta, 0)$ is the rate at which a spark causes release from all activated sites, i.e., whole cell release. For consistency, it must be that

$$\beta M h = \int_0^h W(h, \eta)d\eta + W(h, 0), \tag{43}$$

indicating that the rate at which sites are inactivated is the same as the rate at which sparks are produced.

We can use (42) to determine when whole cell release occurs. Suppose that at time $t = 0$ there is a whole cell release event. Accordingly, at time $t = 0$, all sites are in state S_{100}, i.e. $h = 0$. Thus, we take $p(h, 0) = \delta(h)$.

Now suppose T_w is the random variable for the next time of whole cell calcium release.

N	$=$	10^5	$\frac{\beta N}{k_h}$	$=$	50
$\frac{D}{k_s L^2}$	$=$	0.1	$\frac{\sigma^*}{\theta L}$	$=$	20

Table 2: Parameter values used for the stochastic whole cell model.

It follows that

$$P(T_w < t) = 1 - \int_0^1 p(h,t)dh, \tag{44}$$

so that

$$q(t) = -\int_0^1 p_t(h,t)dh \tag{45}$$

is the probability distribution function for the random variable T_w.

All that remains to do is to specify the transition rate $W(\eta, h)$ and then to find the corresponding solution of (42). We use the information gained from the previous section on the spark to wave transition to specify $W(\eta, h)$. From that discussion (see Eqn. (38)) we determined that a reasonable model for the extent of propagation is

$$P(N_e = n) = (1 - m_0)\exp(n \ln m_0), \tag{46}$$

which suggests that a reasonable model for $W(\eta, h)$ is the exponential distribution

$$W(\eta, h) = -\beta\eta M^2 \ln(m_0)\exp\left(M(\eta - h)\ln(m_0)\right), \qquad 0 < h < \eta \tag{47}$$

and

$$W(\eta, 0) = \beta M \eta \exp(M\eta \ln m_0), \tag{48}$$

where m_0 is a function of η.

To specify m_0, we recall from the previous section that m_0 depends on the two parameters $\delta = \frac{D}{k_s L^2}$, the dimensionless diffusion constant, and $\frac{\sigma}{\theta L}$, the dimensionless release amplitude. Release sites are organized into clusters of IPR's, and at any given time some fraction of these receptors are bound by $[IP_3]$. The amount of calcium released through the cluster is proportional to the number of receptors that participate in the release event. One expects the number of bound receptors to be binomially distributed so that the amount of released calcium is also variable [26]. However, for this model we assume that the number of receptors that participate in each release event is the same, so that the release amount is

$$\sigma = \sigma^* h F, \tag{49}$$

where σ^* is the release amount if the entire cluster is activated, and F represents the fraction of receptors that are bound by $[IP_3]$. Finally, we take $M = NF$, where N is the total number of release sites in the cell.

More detailed models of $[IP_3]$ dependence, for example allowing θ, β, and/or k_h to depend on $[IP_3]$, are possible, but have no substantial effect on the results. Similarly, no particular quantitative relationship with $[IP_3]$ is assigned to F.

The model shows three different types of behavior associated with the shape of the function $W(\eta, 0)$. If F is small, $W(\eta, 0)$ is essentially zero, so that there is no realistic chance

of a whole cell calcium release event. On the other hand, if F is sufficiently large, then with enough sites activated, whole cell release is certain. Finally, there is an intermediate range where whole cell release is possible but not very likely, even if all the available sites are activated.

The function $W(\eta, 0)$ is shown in Fig. 14 for two of these three situations. With $F = 1$ it is seen that for η sufficiently large, $W(\eta, 0) = \eta$, indicating that whole cell release is certain for these values of η. In the intermediate case, with $F = 0.51$, whole cell release is possible, but only if most of the sites are in the activated state. The case where F is small is not shown because $W(\eta, 0)$ is for all practical purposes zero.

Similar differences in behavior can be understood from a plot of the function $W(\eta, h)$, shown in Fig. 15 with $F = 1$ and $N = 100$. For small values of η, $W(\eta, h)$ is essentially zero except near $\eta = h$, indicating that sparks fail to initiate waves. For intermediate values of η, $W(\eta, h)$ is exponential in h, indicating that sparks initiate abortive waves. Finally, for large η, $W(\eta, h) = 0$, indicating that all sparks initiate whole cell release.

Fig. 16 shows examples of the probability distribution function $q(t)$ for three different values of the $[IP_3]$ saturation F ($F = 1.0, 0.85, 0.7$), determined by numerical simulation of equation (42) starting with initial data $p(h, 0) = \delta(h)$. With $F = 0.7$, whole cell release is infrequent and occurs with high variability. At these intermediate values of saturation, whole cell release is possible only if a majority of the sites are activated, but this is prevented from happening by sparks and abortive waves. As F increases, whole cell release becomes more likely and less variable. To illustrate this, the expected release time (solid curve) and its standard deviation (dashed curve) are shown plotted as functions of F in Fig.17. Clearly, both the median time of release and the width of the distribution are decreasing functions of the parameter F. This is exactly the behavior found in [10] using Monte Carlo simulations.

4 Discussion

Whole cell calcium models are based on two assumptions that in many physiological situations are not valid. First, in large cells, whole cell calcium release occurs because of a wave that propagates from release site to site, and when this occurs, calcium is not uniformly distributed throughout the cell, so that the concept of whole cell calcium concentration is essentially meaningless. Second, the whole cell release transient is initiated by a random event, and is therefore not deterministic.

The model for calcium oscillations presented here relies on the assumption that release from a release site is stochastic, depending on the local calcium concentration, and is very rapid, allowing the use of the fire-diffuse-fire model. Other assumptions, such as assuming that there is no calcium exchange with the extracellular environment, or that the calcium release amount is fixed, are not essential to this discussion, and can easily be modified. However, because of the assumption that all waves are initiated by sparks and propagate rapidly compared to the timescale of reactivation, this model does not have self-sustained spatiotemporal patterns such as spirals and target patterns, nor does it have patterns resulting from simultaneous release and coherence resonance described in [31].

In [5, 6], a different way of randomizing the fire-diffuse-fire model was used. There, release occurred when the calcium concentration hit the threshold level θ, which was assumed to

be noisy rather than fixed. In that work, stochastic simulations were used to study the spark-to-wave transition.

One way to relate the approach in [6] to that taken here is to introduce a random variable $\eta = c(x_n, t) - \theta(t)$ and to write a Langevin equation for η,

$$d\eta = c_t(x_n, t)dt + \sqrt{2\Delta dt}\xi(t), \tag{50}$$

where $\xi(t)$ is a Gaussian process with mean zero and variance one, and Δ specifies the variance of the noisy threshold θ. For this Langevin equation, there is the corresponding Fokker-Planck equation describing the evolution of the probability distribution of η,

$$\frac{\partial \rho}{\partial t} = -c_t(x_n, t)\frac{\partial \rho}{\partial \eta} + \Delta \frac{\partial^2 \rho}{\partial \eta^2}. \tag{51}$$

If we assume that at time $t = 0$, $\rho(\eta, 0) = \delta(\eta + \theta_0)$, where θ_0 is the mean of the threshold θ, and we use the absorbing boundary condition, $\rho(0, t) = 0$, then it follows that

$$P_n(t) = 1 - \int_{-\infty}^{0} \rho(\eta, t)d\eta. \tag{52}$$

This definition of $P_n(t)$ should give results quite similar to those with $P_n(t)$ defined by (18), although a detailed comparison has not been done. It is the case, however, that numerical determination of $P_n(t)$ using the definition (52) is an order of magnitude more difficult than using (18), since (52) requires the numerical solution of the partial differential equation (51), rather than the ordinary differential equation (18).

An interesting question is why Hodgkin-Huxley-type models for electrical activity of excitable cells do not suffer from the same flaws as calcium models. (One might argue that they do suffer from the same difficulties. In fact, there is a lot of noisiness in neural networks that is not accounted for by deterministic models. See, for example, [13].) After all, the structure and concepts behind the models are identical. Both are conservation laws of the form

$$\frac{\partial u}{\partial t} = D\nabla^2 u + \text{source terms}, \tag{53}$$

and for both, the sources are spatially discrete fluxes of ions through channels that are stochastic, being either open or closed. Furthermore, for both, the probability of being open or closed is influenced by the local value of the variable u.

The essential mathematical questions are when can one replace the sum of discrete random variables with their average behavior (the law of large numbers), and when can one homogenize a spatially inhomogeneous equation.

The answer is one of quantities and not qualities. First, the electrical forces generated by inhomogeneities of charge are much larger than the chemical forces generated by inhomogeneities of chemical concentrations. Thus, transmembrane potential tends to be much less spatially inhomogeneous than chemical concentrations, and inhomogenieties are smoothed much more rapidly. Indeed the space constant for electrical potential is several orders of magnitude larger than for chemical concentrations, being typically 0.5 cm for axons compared with 0.5 μm for calcium [34]. Second, calcium channels tend to occur in clusters and

so the amount of calcium released per release site is relatively large, compared to the amount of sodium (say), through a voltage controlled sodium channel. The law of large numbers works much better for a large number of small amplitude events than for a small number of large amplitude events. Thus, equations governing electrical behavior of membranes are much better candidates for homogenization and the application of the law of large numbers than are equations governing the dynamics of calcium.

The broader implication of this work is that there are significant cellular events for which deterministic models are not appropriate. For these, there is a need for a new modeling paradigm, assessing the probability of the event under different parametric conditions. Here we examined only single cell events, however, this approach could be of significant interest at the multicellular/organ level when applied to life threatening transitions.

References

[1] N. L. Allbritton, T. Meyer, and L. Stryer. Range of messenger action of calcium ion and inositol 1,4,5-trisphosphate. *Science*, 258:1812–1815, 1992.

[2] A. E. Bugrim, A. M. Zhabotinsky, and I. R. Epstein. Calcium waves in a model with a randomly spatially discrete distribution of Ca^{2+} release sites. *Biophys. J.*, 73:2897–2906, 1997.

[3] H. Cheng, W. J. Lederer, and M. B. Cannell. Calcium sparks: Elementary events underlying excitation-contraction coupling in heart muscle. *Science*, 262:740–744, October 1993.

[4] S. Coombes. The effect of ion pumps on the speed of travelling waves in the fire-diffuse-fire model of Ca^{2+} release. *Bull. Math. Biol.*, 63:1–20, 2001.

[5] S. Coombes, R. Hinch, and Y. Timofeeva. Receptors, sparks and waves in a fire-diffuse-fire framework for calcium release. *Progress in Biophysics and Molecular Biology*, 85:197–216, 2004.

[6] S. Coombes and Y. Timofeeva. Sparks and waves in a stochastic fire-diffuse-fire model of Ca^{2+} release. *Phys. Rev. E*, 68:021915, 2003.

[7] D. R. Cox. *Renewal Theory.* Chapman and Hall, New York, 1962.

[8] S. P. Dawson, J. Keizer, and J. E. Pearson. Fire-diffuse-fire model of dynamics of intracellular calcium waves. *Proc. Natl. Acad. Sci. USA*, 96:6060–6063, May 1999.

[9] M. Falcke. Buffers and oscillations in intracellular Ca^{2+} dynamics. *Biophys. J.*, 84:42–56, 2003.

[10] M. Falcke. On the role of stochastic channel behavior in intracellular Ca^{2+} dynamics. *Biophys. J.*, 84:42–56, 2003.

[11] M. Falcke. Reading the patterns in living cells - the physics of Ca^{2+} signalling. *Adv. Phys.*, 53:255–440, 2004.

[12] C. J. Favre, J. Schrenzel, J. Jacquet, D. P. Lew, and K. H. Krause. Highly supralinear feedback inhibition of Ca^{2+} uptake by the Ca^{2+} load of intracellular stores. *J Biol Chem.*, 271(25):14925–30, 1996.

[13] R. F. Fox. Stochastic versions of the Hodgkin-Huxley equations. *Biophys J.*, 72:2068–2074, 1997.

[14] C. W. Gardiner. *Handbook of Stochastic Methods*. Springer, 2nd edition, 1985.

[15] L. T. Izu, W. G. Wier, and C. W. Balke. Evolution of cardiac calcium waves from stochastic calcium sparks. *Biophys. J.*, 80:103–120, 2001.

[16] J. P. Keener and J. Sneyd. *Mathematical Physiology*. Springer-Verlag, New York, 1998.

[17] J. Keizer and G. DeYoung. Simplification of a realistic model of IP_3-induced Ca^{2+} oscillations. *J. Theor. Biol.*, 166:431–442, 1994.

[18] J. Keizer and G. D. Smith. Spark-to-wave transition: saltatory transmission of calcium waves in cardiac myocytes. *Biophys. Chem.*, 72:87–100, 1998.

[19] J. Keizer, G. D. Smith, S. Ponce-Dawson, and J. E. Pearson. Saltatory propagation of Ca^{2+} waves by Ca^{2+} sparks. *Biophys. J.*, 75:595–600, 1998.

[20] Y.-X. Li and J. Rinzel. Equations for $InsP_3$ receptor-mediated ca^{2+} oscillations derived from a detailed kinetic model: a Hodgkin-Huxley like formalism. *Journal of Theoretical Biology*, 166:461–473, 1994.

[21] J. Marchant and I. Parker. Role of elementary Ca^{2+} puffs in generating repetitive Ca^{2+} oscillations. *EMBO J.*, 20:65–76, 2001.

[22] I. Parker, J. Choi, and Y. Yao. Elementary events of $InsP_3$-induced Ca^{2+} liberation in *xenopus* oocytes: hot spots, puffs and blips. *Cell Calcium*, 20(2):105–121, 1996.

[23] J. E. Pearson and S. Ponce-Dawson. Crisis on skid row. *Physica A*, 257:141–148, 1998.

[24] A. Sherman and J. Rinzel. Model for synchronization of pancreatic β-cells by gap junction coupling. *Biophys. J.*, 59:547–559, 1991.

[25] A. Sherman, J. Rinzel, and J. Keizer. Emergence of organized bursting in clusters of pancreatic β-cells by channel sharing. *Biophys. J.*, 54:411–425, 1988.

[26] J. W. Shuai and P. Jung. Stochastic properties of Ca^{2+} release of inositol 1,4,5-trisphosphate receptor clusters. *Biophys. J.*, 83:87–97, 2002.

[27] G. Smith, L. Dai, R. Miura, and A. Sherman. Asymptotic analysis of buffered calcium diffusion near a point source. *SIAM J. Appl. Math.*, 61:1816–1838, 2001.

[28] J. Sneyd. *Tutorials in Mathematical Biosciences II*, volume 187 of *Lecture Notes in Mathematics*, chapter Mathematical modeling of calcium dynamics and signal transduction. Springer, 2005.

[29] R. Thul and M. Falcke. Release currents of IP_3 receptor channel clusters and concentration profiles. *Biophys. J.*, 86:2660–2673, 2004.

[30] R. Thul and M. Falcke. Stability of membrane bound reactions. *Phys. Rev. Letts.*, 93, 2004.

[31] Y. Timofeeva and S. Coombes. Wave bifurcation and propagation failure in a model of calcium release. *J. Math. Biol.*, 47:249–269, 2003.

[32] W. G. Wier and C. W. Balke. Ca^{2+} release mechanisms, Ca^{2+} sparks, and local control of excitation-contraction coupling in normal heart muscle. *Circ. Res.*, 85:770–776, 1999.

[33] G. W. De Young and J. Keizer. A single pool $[IP_3]$-receptor based model for agonist stimulated $[Ca^{++}]$ oscillations. *Proc. Natl. Acad. Sci. USA*, 89:9895–9899, 1992.

[34] A. Zador and C. Koch. Linearized models of calcium dynamics: formal equivalence to the cable equation. *J. Neurosci.*, 14:4705–4715, 1994.

5 Figures

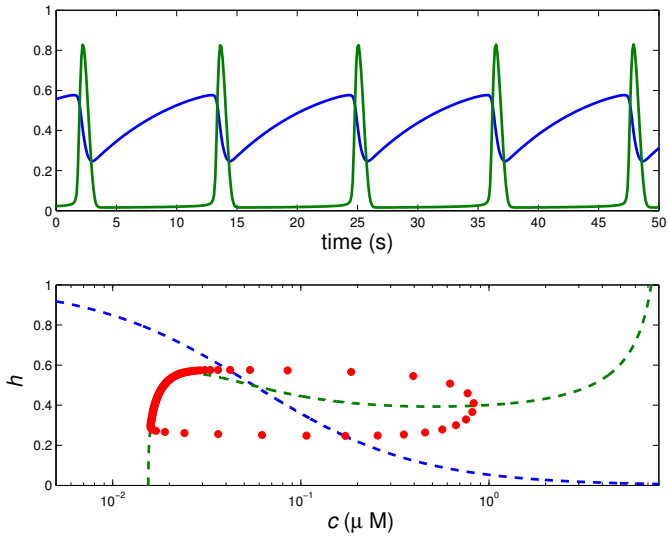

Figure 1: Calcium oscillations in the whole cell model (5-11) using parameter values from Table 1; upper panel: time course, lower panel: phase portrait, with nullclines shown as dashed curves and h-c trajectory shown as circular dots.

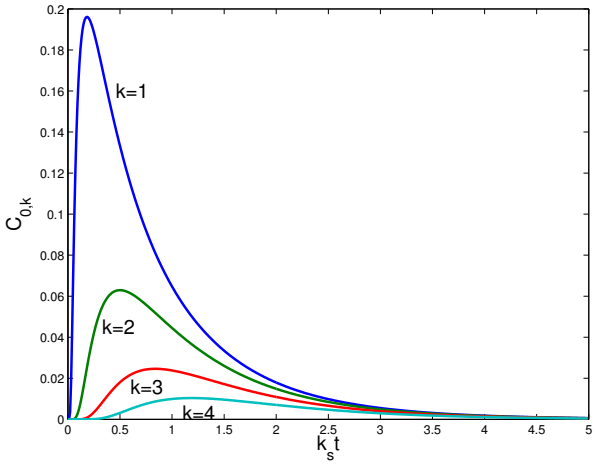

Figure 2: Fundamental solution of (12), $C_{0,k}(t)$, plotted as a function of $k_s t$ for $\delta = 2.0$ and for $k = 1, 2, 3, 4$.

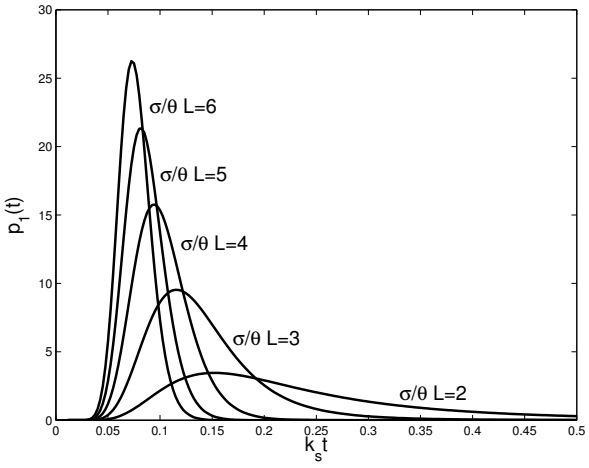

Figure 3: Probability distribution function $p_1(t)$ for the firing time at site 1, plotted for $\frac{\sigma}{\theta L} = 2, 3, 4, 5, 6$, with $\delta = 2.0$.

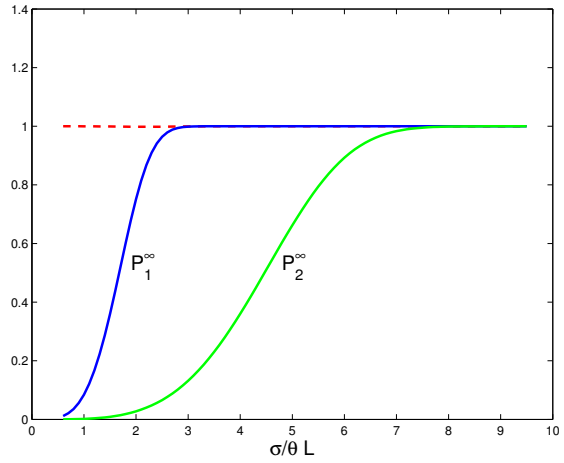

Figure 4: Probability of firing at site 1 (P_1^∞) and site 2 (P_2^∞) as a result of a single release event at site 0 only, plotted as functions of $\frac{\sigma}{\theta L}$, with $\delta = 2$. The upper unlabeled curve is the probability that release at site 1 precedes release at site 2, $P(t_1 < t_2|\text{site 1 release occurs})$, and is quite close to 1.

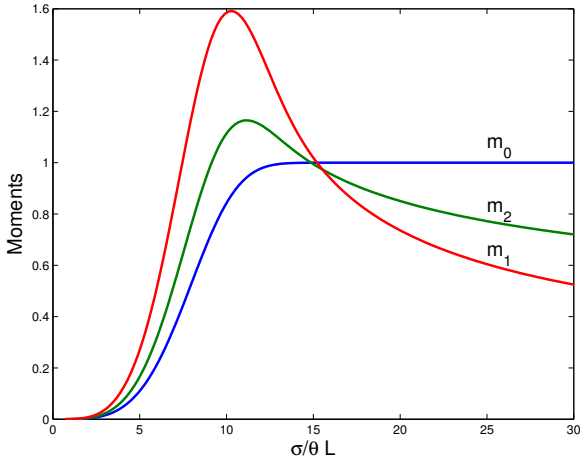

Figure 5: The moments m_0, m_1 and m_2 of $p_1(t)$ as functions of $\frac{\sigma}{\theta L}$ with $\delta = 0.1$.

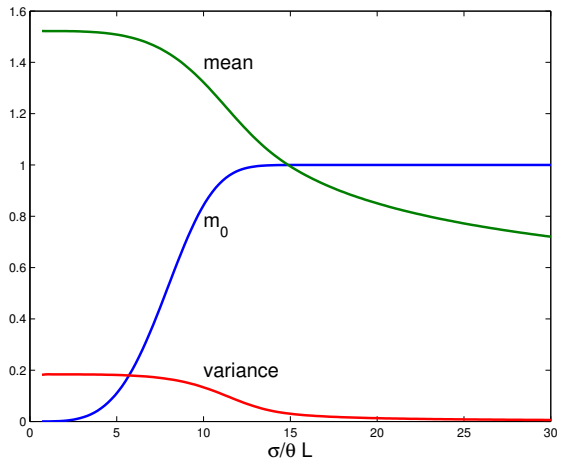

Figure 6: The curves m_0, $\frac{m_1}{m_0}$ (the mean) and $\frac{m_2}{m_0} - \left(\frac{m_1}{m_0}\right)^2$ (the variance) of $\frac{p_1(t)}{P_1^\infty}$ as functions of $\frac{\sigma}{\theta L}$ with $\delta = 0.1$.

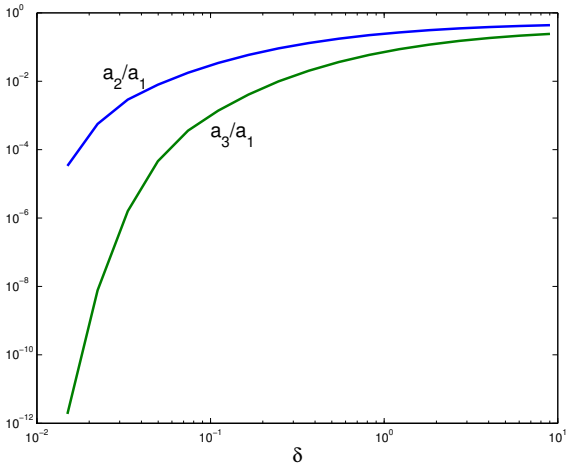

Figure 7: Plot of the ratios $\frac{a_2}{a_1}$ and $\frac{a_3}{a_1}$ as functions of δ on a log-log plot.

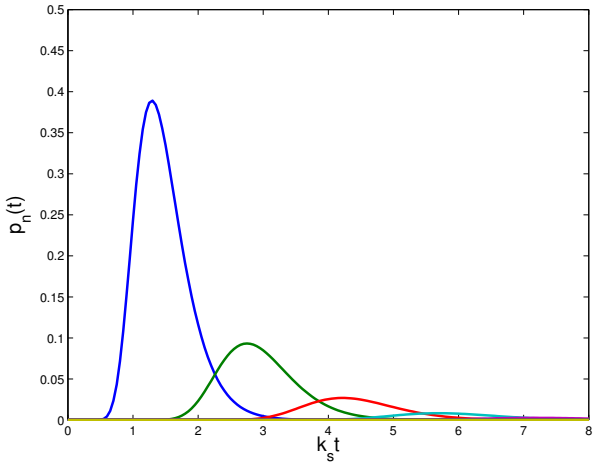

Figure 8: Solutions $p_n(t)$ of the recurrence equation (31) for $n = 1, \cdots, 5$ with $\delta = 0.1$ and $\frac{\sigma}{\theta L} = 7$. For this plot, $m_0 = 0.36$, corresponding to an abortive wave.

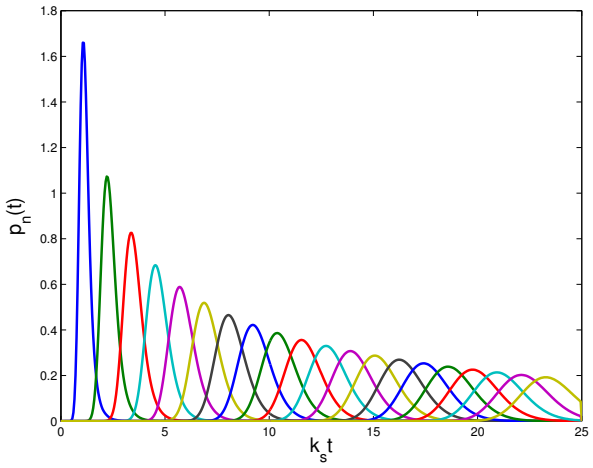

Figure 9: Solutions $p_n(t)$ of the recurrence equation (31) for $n = 1, \cdots, 20$ with $\delta = 0.1$ and $\frac{\sigma}{\theta L} = 12$. For this plot, $m_0 = 0.9775$, for which propagation is sustained for a long distance.

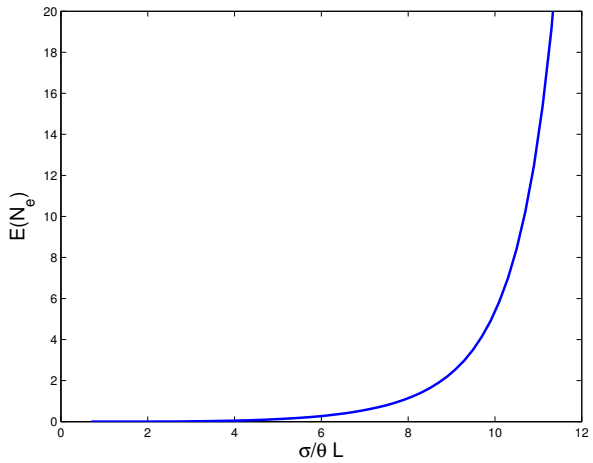

Figure 10: Expected number of release events $E(N_e)$ plotted as a function of $\frac{\sigma}{\theta L}$ with $\delta = 0.1$.

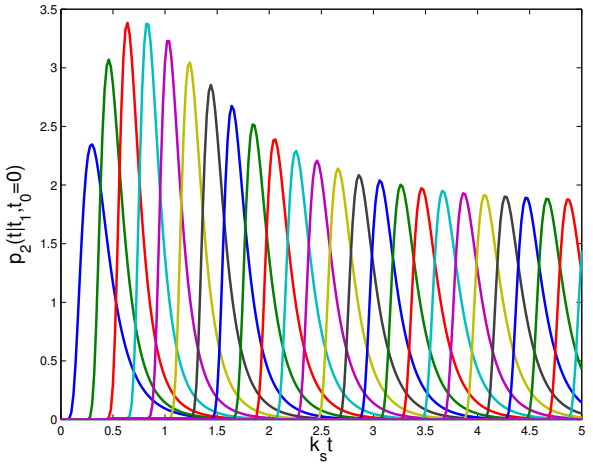

Figure 11: The conditional release function $p_2(t|t_1, t_0 = 0)$ for 24 different values of t_1 ranging from 0 to $4.6k_s$, with $\delta = 1.0$ and $\frac{\sigma}{\theta L} = 2.0$.

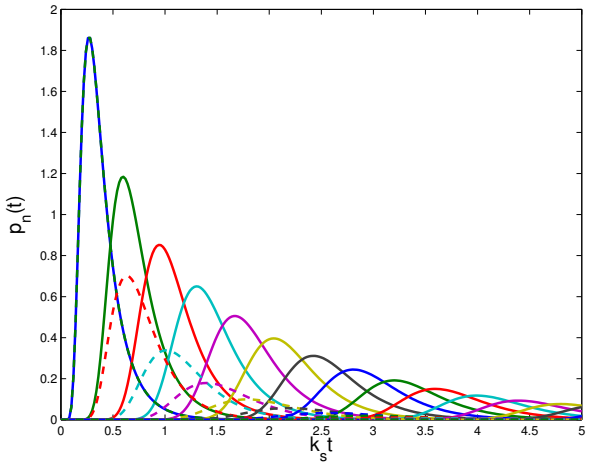

Figure 12: The sequence of functions $p_n(t)$ for $n = 1, \cdots, 14$ with $\delta = 1.0$ and $\frac{\sigma}{\theta L} = 2.0$ found as solutions of the two-step recurrence equation (40). The dashed curves are the solutions of renewal equation (31) for the same parameter values.

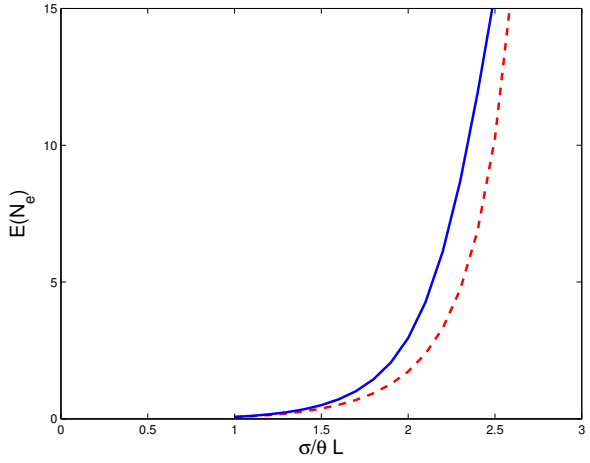

Figure 13: Expected number of release events $E(N_e)$ plotted as a function of $\frac{\sigma}{\theta L}$ with $\delta = 1.0$. The dashed curve shows the result using the formula (39) which assumes that release depends on nearest neighbor interactions only.

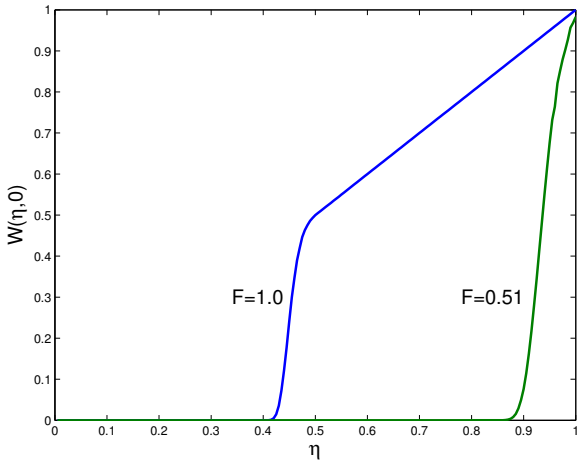

Figure 14: The function $W(\eta, 0)$ plotted as a function of η for two different values of F. Other parameter values are given in Table 2.

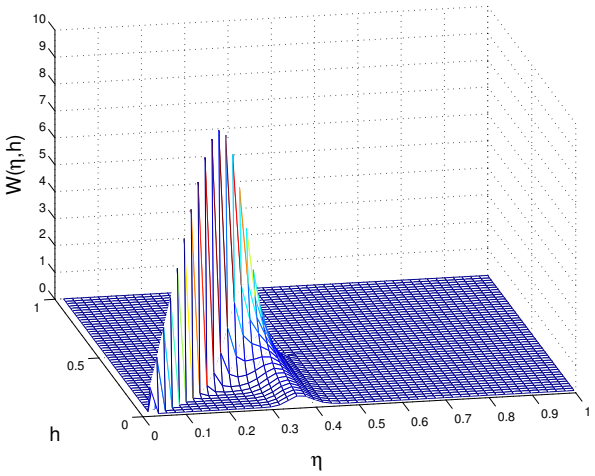

Figure 15: The function $W(\eta, h)$ plotted as a function of η and h for $F = 1$ and $N = 100$, with other parameter values given in Table 2.

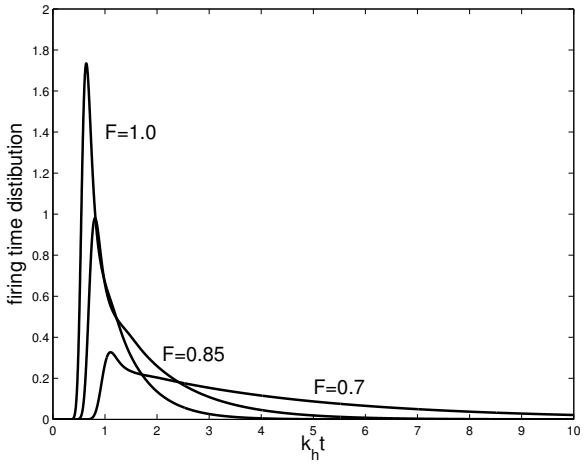

Figure 16: Probability distribution function for the time of whole cell calcium release, shown for 3 different values of $[IP_3]$ saturation $F = 0.7, 0.85, 1.0$. Other parameter values are given in Table 2.

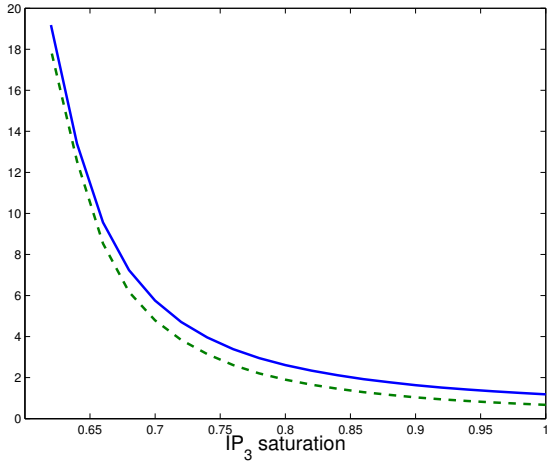

Figure 17: The expected time of whole cell calcium release (solid curve) and the standard deviation (dashed curve), in units of dimensionless time $k_h t$, shown plotted as functions of $[IP_3]$ saturation F.